Reconstructing small perturbations in electrical admittivity at low frequencies

2014 Inverse Problems 30 035006

(http://iopscience.iop.org/0266-5611/30/3/035006)

IOP Publishing Inverse Problems

Inverse Problems **30** (2014) 035006 (18pp) doi:10.1088/0266-5611/30/3/035006

Reconstructing small perturbations in electrical admittivity at low frequencies

Sungwhan Kim[1] **and Alexandru Tamasan**[2]

[1] Division of Liberal Arts, Hanbat National University, Korea
[2] Department of Mathematics, University of Central Florida, USA

E-mail: sungwhan@hanbat.ac.kr and tamasan@math.ucf.edu

Received 19 August 2013, revised 25 December 2013
Accepted for publication 7 January 2014
Published 12 February 2014

Abstract

We present a method to recover small perturbations from constants in electrical conductivity σ and relative (to the air's) permittivity ϵ of a body, from electrical measurements at low frequencies at the boundary. The method is based on the asymptotic expansion of the frequency differential of the Neumann-to-Dirichlet map with respect to both frequency and perturbation size. To show its feasibility, we implement the method on two numerical experiments for a complete electrode model.

Keywords: electrical impedance tomography, small perturbation, frequency differential

(Some figures may appear in colour only in the online journal)

1. Introduction

Electrical impedance tomography (EIT) is the imaging technique in which the electrical conductivity σ and permittivity ε of a body Ω is to be recovered from knowledge of electrical currents and voltages at its boundary Γ. In this study we have in mind excitations at low frequency ν of order of 1 kHz. In the imaginary part of the admittivity $\sigma + \mathrm{i}\nu\varepsilon$ we assume a permittivity ϵ scaled relative to the permittivity ε_{air} of air, i.e.

$$\epsilon := \varepsilon/\varepsilon_{\text{air}}, \quad \omega := \nu\epsilon_{\text{air}}.$$

Since $\epsilon_{\text{air}} \approx 8.8 \times 10^{-12}$ F m^{-1} and $\nu \approx 1$ kHz, the values of ω are numerically small of order $O(10^{-8})$. Note that the susceptivity $\nu\varepsilon$ is invariant under this scaling.

Most generally formulated by Calderón [8] at $\omega = 0$ (when only σ has been sought), the problem has seen a tremendous development both on the mathematics and engineering facet with breakthrough results in [1, 7, 25, 26, 27, 37] complemented by important contributions as reviewed in [2, 4, 9, 15, 39]. At zero frequency direct nonlinear approaches that use the

complex geometrical optic solutions (CGOs) have been proposed in [21, 23, 24, 30] based on the reconstruction methods in [1, 3, 6, 22, 27]. At a fixed frequency ω, the Dirichlet-to-Neumann map uniquely determines the admittivity $\sigma + \mathrm{i}\nu\epsilon$. This is true in dimensions 2 due to the result in [7], also in [10] for sufficiently small susceptivity $\nu\epsilon$. Note that we do not assume a small susceptivity here since the scaling above leaves the susceptivity invariant.

In three dimensions and higher the results in [26, 37] seem to extend to the complex coefficient case provided *a priori* information on admittivity and its normal derivative at the boundary is known. An algorithm for two dimensional complex admittivity based on [10] has been proposed recently in [11].

At low frequencies the effect of susceptivity cannot be neglected and working with a complex valued voltage potential becomes necessary. Practitioners are able to measure both the magnitude and the phase of the complex valued potential at the boundary [5, 28, 31, 36, 38]. At low frequencies the information about permittivity is mainly carried by the imaginary part of the voltage potential [20]. The results in section 2 (see remark 2.3) identifies the needed information and how it can be obtained in two different ways:

- on the one hand one can use the real part of a suitably scaled voltage potential. This is the approach we took in the numerical experiments here;
- on the other hand one can use the difference in voltages at two distinct frequencies. This is a fairly recent development known as the frequency difference/differential EIT (fdEIT) [12, 13, 16, 18, 19, 33, 34].

In general, the methods based on subtraction of two boundary data seem to be more robust due to the cancellation of instrumentation errors in the data; this has also been observed in fdEIT [33, 34].

We work under the assumptions that $\sigma = \sigma(x)$ and $\epsilon = \epsilon(x)$. In reality they also vary with frequency ω. For data collected at a single frequency this work interprets the conductivity and permittivity as the ones corresponding to that single frequency. For data collected at two different but comparable frequencies, we assume that σ and ϵ do not vary with frequency at comparable values.

The mathematical formulation considers a time harmonic current $g\cos(\omega t)$ being injected into an object Ω through surface electrodes to induce a complex voltage potential u_ω solution of the Neumann problem:

$$\begin{cases} \nabla\cdot(\sigma + \mathrm{i}\omega\epsilon)\nabla u_\omega = 0, & \text{in} \quad \Omega, \\ -(\sigma + \mathrm{i}\omega\epsilon)\frac{\partial u_\omega}{\partial \mathbf{n}} = g, & \text{on} \quad \Gamma, \\ \int_\Gamma u_\omega \,\mathrm{d}s = 0, \end{cases} \tag{1}$$

for some real valued function $g \in H^{-1/2}(\Gamma)$. Assuming $1/c \leqslant \sigma \leqslant c$ for some $c > 0$, the unique solution u_ω of (1) is measured at the boundary to define the Neumann-to-Dirichlet map $\mathcal{N}_{\gamma_\omega} : H_0^{-1/2}(\Gamma) \to H_0^{1/2}(\Gamma)$ by

$$\mathcal{N}_{\gamma_\omega} : g \mapsto u_\omega|_\Gamma. \tag{2}$$

Here $H_0^{1/2}(\Gamma)$ is the space of traces with vanishing mean at the boundary of functions in $H^1(\Omega)$, and $H_0^{-1/2}(\Gamma)$ is the dual of $H_0^{1/2}(\Gamma)$ with respect to the $L^2(\Gamma)$-inner product.

Despite the transparent usefulness in medical diagnostics, the quantities behind the fdEIT images are not yet fully understood. However, for $\Omega \subset \mathbb{R}^n$, $n \geqslant 3$, $\sigma \in C^{1,1}(\overline{\Omega})$ constant near the boundary and $\epsilon \in C_0^{1,1}(\overline{\Omega})$ the frequency differential at $\omega = 0$ of the Dirichlet-to-Neumann map uniquely determines the quantity

$$Q[\sigma, \epsilon] := \nabla\cdot(\nabla\epsilon - \epsilon\nabla\ln\sigma)/\sigma \tag{3}$$

as shown by the authors in [20]. The method is non-constructive and relies on CGOs. Since knowledge of the Dirichlet-to-Neumann map is equivalent to knowledge of the Neumann-to-Dirichlet map, one can conclude that the quantity Q is also uniquely determined by $\frac{\mathrm{d}}{\mathrm{d}\omega}\big|_{\omega=0}\mathcal{N}_{\gamma_\omega}$.

In this paper we give a reconstruction method for the linearized problem of fdEIT about some known constant conductivity σ_b, and permittivity ϵ_b, which quantitatively recovers the perturbations. The method proposed is not based on CGOs and applies to models in two or higher dimensions. To exhibit the error estimates due to the linearization, we consider

$$\sigma_t := \sigma_b + t\tilde{\sigma}, \quad \epsilon_t := \epsilon_b + t\tilde{\epsilon}, \quad \gamma_\omega^t := \sigma_t + \mathrm{i}\omega\epsilon_t, \tag{4}$$

for some $\tilde{\sigma}, \tilde{\epsilon} \in L^\infty(\Omega)$ with compact support in Ω, and $t \geqslant 0$ sufficiently small. While $\tilde{\sigma}$ and $\tilde{\epsilon}$ are not known, we assume they are *a priori* bounded by some known $r \geqslant 0$:

$$\|\tilde{\sigma}\|_\infty \leqslant r \quad \text{and} \quad \|\tilde{\epsilon}\|_\infty \leqslant r, \tag{5}$$

where $\|\cdot\|_\infty$ denotes the $L^\infty(\Omega)$-norm.

Since $(\tilde{\sigma}, \tilde{\epsilon})|_\Gamma$ are assumed known (in fact vanishing), the derivative

$$\left.\frac{\mathrm{d}Q[\sigma_t, \epsilon_t]}{\mathrm{d}t}\right|_{t=0^+} = \frac{\epsilon_b}{\sigma_b}\Delta\left(\frac{\tilde{\epsilon}}{\epsilon_b} - \frac{\tilde{\sigma}}{\sigma_b}\right),$$

recovers the quantity

$$\delta Q := \left(\frac{\tilde{\epsilon}}{\epsilon_b} - \frac{\tilde{\sigma}}{\sigma_b}\right). \tag{6}$$

For sufficiently small t, in here we reconstruct $t[\delta Q]$ from the frequency differential of an appropriately scaled $\mathcal{N}_{\gamma_\omega^t}$. The method is based on the following result, which is proved in section 3.

Theorem 1.1. *Let σ_t, ϵ_t, and γ_ω^t in (4) satisfy (5). Let $t_0 \leqslant 1$ be sufficiently small such that*

$$1/c \leqslant \sigma_t \leqslant c, \tag{7}$$

for some $c > 0$ independent of $0 \leqslant t \leqslant t_0$. Let $f, g \in H_0^{-1/2}(\Gamma)$, and $\phi_f, \phi_g \in H^1(\Omega)$ be the harmonic functions with mean vanishing traces on Γ, which satisfy $-\sigma_b\frac{\partial\phi_f}{\partial\mathbf{n}}\big|_\Gamma = f$, respectively $-\sigma_b\frac{\partial\phi_g}{\partial\mathbf{n}}\big|_\Gamma = g$. Then, with δQ the quantity in (6), we have

$$\int_\Omega [\delta Q]\nabla\phi_g\cdot\nabla\phi_f\,\mathrm{d}x = \lim_{t\to 0^+}\frac{1}{t}\left\langle \left.\frac{\mathrm{d}}{\mathrm{d}\omega}\right|_{\omega=0}\left\{\left(\frac{\omega}{\sigma_b} - \frac{\mathrm{i}}{\epsilon_b}\right)\mathcal{N}_{\gamma_\omega^t}g\right\},\ f\right\rangle_\Gamma, \tag{8}$$

where $\langle\cdot,\cdot\rangle_\Gamma$ denotes the pairing of functions in $H^{\pm 1/2}(\Gamma)$ with respect to the $L^2(\Gamma)$-inner product.

Since products of gradients of harmonic function is dense in $L^2(\Omega)$ (as originally noted by Calderón in his linearization approach in [8]), the right-hand side of (8) for appropriate choices of f and g uniquely determines (the Fourier transform of) δQ in (6). However, in the method proposed here we do not use the density of gradients of harmonic functions above. Instead, we propose a method in which the resolution in the image is predetermined by the number (of combinations) of electrodes, where in each pixel the unknown δQ is assumed constant. The method and its numerical implementation are tailored for the complete electrode model in [35].

While the nonlinear approach in [20] shows that $\frac{\mathrm{d}}{\mathrm{d}\omega}\big|_{\omega=0}\mathcal{N}_{\gamma_\omega}$ recovers Q, in here we show that the linearization of $\frac{\mathrm{d}}{\mathrm{d}\omega}\big|_{\omega=0}\mathcal{N}_{\gamma_\omega}$ recovers the linearization of Q. This gives a natural interpretation of (6), whose support has been recovered previously in [12].

A key feature of authors' result in [20] is the analytic dependence in ω of the voltage potential, for frequencies satisfying

$$\left\|\frac{\omega\epsilon}{\sigma}\right\|_\infty < 1, \tag{9}$$

which allows for a recurrence type decoupling in the real and imaginary part of u_ω. The analogous result (proven in the appendix) holds for the solution of the Neumann problem (1), and allows to explicit the asymptotic expansion of the data $\frac{\mathrm{d}}{\mathrm{d}\omega}\big|_{\omega=0}\left\{\left(\frac{\omega}{\sigma_b}-\frac{\mathrm{i}}{\epsilon_b}\right)\mathcal{N}_{\gamma_\omega^t}g\right\}$ with an error estimate; it also explains why the harmonic functions appearing in the left-hand side of (8) are independent on the permittivity. The hypothesis (9) is meaningful to biomedical applications such as in [32]. According to experimental values at 10 kHz for a variety of biological tissues [29], the left-hand side of (9) has a maximum of 0.528 achieved in the tissue of the heart.

In section 4 we present a method which reconstructs $t(\delta Q)$ from boundary voltages. We use the complete electrode model in [35] to obtain (approximate) solutions of the Neumann problem (1).

In section 5 we first adapt Calderón's original arguments to recover the small perturbation $t\tilde{\sigma}$ from the real part $\Re(u_\omega)$. In combination with knowledge of $t(\delta Q)$ we can also recover $t\tilde{\epsilon}$ separately. Different from the result in [14], which recovers the support of the perturbation in admittivity, our method here provides a quantitative reconstruction.

The method is implemented in two numerical experiments in section 6. We conclude with a series of remarks.

2. Analytic dependence in frequency

In this section we present the analytic dependence in ω of the complex valued solutions $u_\omega \in H^1(\Omega)$ of (1). The admittivity need not be a small perturbation from constant. Due to the frequency dependence in the Neumann boundary condition the estimates (while similar to the ones in [20, theorem 3.1]) requires a different proof. To preserve the flow of exposition of the inverse problem, the details are included in the appendix.

Theorem 2.1. *Let $\sigma, \epsilon \in L^\infty(\Omega)$ with σ satisfying (7) for some $c > 0$. Assume that ω lies in the frequency range (9). Then the Neumann problem (1) has a unique solution $u_\omega \in H^1(\Omega)$, whose real part $v_\omega = \Re(u_\omega)$, and imaginary part $h_\omega = \Im(u_\omega)$ satisfy the series representation*

$$v_\omega(x) = \sum_{n=0}^{\infty} v_{2n}(x)\omega^{2n}, \quad h_\omega(x) = \sum_{n=0}^{\infty} h_{2n+1}(x)\omega^{2n+1}, \tag{10}$$

with the convergence in the $H^1(\Omega)$-sense. Moreover, v_0 solves

$$\begin{cases} \nabla\cdot(\sigma\nabla v_0) = 0, & \text{in} \quad \Omega, \\ -\sigma\frac{\partial v_0}{\partial \mathbf{n}} = g, & \text{on} \quad \Gamma, \\ \int_\Gamma v_0\,\mathrm{d}s = 0, \end{cases} \tag{11}$$

and, for $k = 0, 1, 2, \ldots$, the following recurrences hold:

$$\begin{cases} \nabla\cdot(\sigma\nabla h_{2k+1}) = -\nabla\cdot(\epsilon\nabla v_{2k}), & \text{in} \quad \Omega, \\ \nabla\cdot(\sigma\nabla v_{2k+2}) = \nabla\cdot(\epsilon\nabla h_{2k+1}), & \text{in} \quad \Omega, \\ -\sigma\frac{\partial h_{2k+1}}{\partial \mathbf{n}} = (-1)^{k+1}\left(\frac{\epsilon}{\sigma}\right)^{2k+1} g, & \text{on} \quad \Gamma, \\ -\sigma\frac{\partial v_{2k+2}}{\partial \mathbf{n}} = (-1)^{k+1}\left(\frac{\epsilon}{\sigma}\right)^{2k+2} g, & \text{on} \quad \Gamma, \\ \int_\Gamma v_{2k+2}\,\mathrm{d}s = \int_\Gamma h_{2k+1}\,\mathrm{d}s = 0. \end{cases} \tag{12}$$

As a corollary, we can now clarify the operator appearing in the right-hand side of (8).

Corollary 2.2. *Let $\sigma, \epsilon \in L^\infty(\Omega)$, with $1/c \leqslant \sigma \leqslant c$, for some $c > 0$. For $g \in H^{1/2}(\Gamma)$ real valued we have*

$$\frac{\mathrm{d}}{\mathrm{d}\omega}\bigg|_{\omega=0} \left\{ \left(\frac{\omega}{\sigma_b} - \frac{\mathrm{i}}{\epsilon_b} \right) \mathcal{N}_{\gamma_\omega} g \right\} = \frac{v_0}{\sigma_b} + \frac{h_1}{\epsilon_b}, \tag{13}$$

where $v_0 \in H^1(\Omega)$ solves (11), and h_1 solves

$$\begin{cases} \nabla \cdot (\sigma \nabla h_1) = -\nabla \cdot (\epsilon \nabla v_0), & \text{in} \quad \Omega, \\ \sigma \frac{\partial h_1}{\partial \mathbf{n}} = \left(\frac{\epsilon}{\sigma} \right) g, & \text{on} \quad \Gamma, \\ \int_\Gamma h_1 \, \mathrm{d}s = 0. \end{cases} \tag{14}$$

Proof. From theorem 2.1 a straightforward calculation shows that

$$\left(\frac{\omega}{\sigma_b} - \frac{\mathrm{i}}{\epsilon_b} \right) \mathcal{N}_{\gamma_\omega} g = -\mathrm{i} \frac{v_0}{\epsilon_b} + \omega \left(\frac{v_0}{\sigma_b} + \frac{h_1}{\epsilon_b} \right) + \omega^2 \tilde{R}(\omega). \tag{15}$$

Moreover, a geometric series summation using the estimates (A.7) and (A.8) in the appendix show that

$$|\tilde{R}(\omega)|_{1/2} \leqslant M ||g||_{-1/2} \left\| \frac{\epsilon}{\sigma} \right\|_\infty^2 \left(1 - \left\| \frac{\epsilon \omega}{\sigma} \right\|_\infty \right)^{-1}, \tag{16}$$

for a constant M which depends on c and Ω only. □

Recall that at low frequencies we work with $\omega = O(10^{-8})$. The following note explains what information obtained from the voltage potential at the boundary is needed in our linearization approach.

Remark 2.3. From the asymptotic formula (15), the right-hand side of (13) can be recovered from boundary data in two different ways:

- For $\omega_1, \omega_2 = O(\omega)$ with $\omega_1 \neq \omega_2$ one can use a difference quotient to get
$$\frac{v_0}{\sigma_b} + \frac{h_1}{\epsilon_b} = \frac{1}{\omega_2 - \omega_1} \left[\left(\frac{\omega}{\sigma_b} - \frac{\mathrm{i}}{\epsilon_b} \right) \mathcal{N}_{\gamma_\omega} g \right]_{\omega_1}^{\omega_2} + O(\omega). \tag{17}$$
- Upon one division by ω and then taking the real part in (15), we have
$$\frac{v_0}{\sigma_b} + \frac{h_1}{\epsilon_b} = \Re \left\{ \left(\frac{1}{\sigma_b} - \frac{\mathrm{i}}{\omega \epsilon_b} \right) \mathcal{N}_{\gamma_\omega} g \right\} + O(\omega). \tag{18}$$

In fdEIT one would use the boundary data as in (17). In the numerical experiments in section 6, we use the formula (18).

3. Proof of theorem 1.1

In this section we denote by $\| \cdot \|_{\pm 1/2}$ the norm in $H^{\pm 1/2}(\Gamma)$, by $\| \cdot \|_{\pm 1}$ the norm in $H^{\pm 1}(\Omega)$, and by $\| \cdot \|$ the norm in $L^2(\Omega)$. We make use several times of the classical estimate in the Neumann problem, which we state without proof below.

Proposition 3.1. *Let $F \in H^{-1}(\Omega)$, $g \in H_0^{-1/2}(\Gamma)$ and $\sigma \in L^\infty(\Omega)$ satisfying (7) for some $c > 0$. Let $v \in H^1(\Omega)$ be the unique solution of the Neumann problem*

$$\begin{cases} \nabla \cdot (\sigma \nabla v) = F, & \text{in} \quad \Omega, \\ -\sigma \frac{\partial v}{\partial \mathbf{n}} = g, & \text{on} \quad \Gamma, \\ \int_\Gamma v \, \mathrm{d}s = 0. \end{cases}$$

Then there exists a constant $M > 0$, dependent only on Ω and c, such that

$$\|v\|_1 \leqslant M(\|g\|_{-1/2} + \|F\|_{-1}). \tag{19}$$

To simplify notation, for the rest of the proof in this section we will drop the vanishing mean normalizing condition from the Neumann problems below, although it is always tacitly assumed.

Recall the notations in (4), and the fact that σ_t satisfies (7) for a constant $c > 0$ independent of $0 \leqslant t \leqslant t_0$. By possibly replacing the constant c by $\epsilon_b + r$, without loss of generality we also assume

$$\|\epsilon_t\|_\infty \leqslant c, \quad \text{for} \quad 0 \leqslant t \leqslant t_0 \leqslant 1. \tag{20}$$

Since we no longer use the series but rather the formula (13), and in order to emphasize dependence in t without cluttering notation, we let $v_t \in H^1(\Omega)$ denote the solutions to

$$\begin{cases} \nabla \cdot (\sigma_t \nabla v_t) = 0, & \text{in} \quad \Omega, \\ -\sigma_t \frac{\partial v_t}{\partial \mathbf{n}} = g, & \text{on} \quad \Gamma, \end{cases} \tag{21}$$

and $h_t \in H^1(\Omega)$ denote the solution of

$$\begin{cases} \nabla \cdot (\sigma_t \nabla h_t) = -\nabla \cdot (\epsilon_t \nabla v_t), & \text{in} \quad \Omega, \\ \sigma_t \frac{\partial h_t}{\partial \mathbf{n}} = \frac{\epsilon_t}{\sigma_t} g, & \text{on} \quad \Gamma. \end{cases} \tag{22}$$

Then, according to (13),

$$\frac{\mathrm{d}}{\mathrm{d}\omega}\bigg|_{\omega=0} \left(\frac{\omega}{\sigma_b} - \frac{\mathrm{i}}{\epsilon_b}\right) \mathcal{N}_{\gamma_\omega^t} g = \left(\frac{v_t}{\sigma_b} + \frac{h_t}{\epsilon_b}\right). \tag{23}$$

For $g, f \in H^{1/2}$ recall that ϕ_g, ϕ_f are the harmonic functions with traces of vanishing mean on Γ that satisfy the Neumann conditions $-\sigma_b \frac{\partial \phi_g}{\partial \mathbf{n}} = g$, respectively $-\sigma_b \frac{\partial \phi_f}{\partial \mathbf{n}} = f$. Note that ϕ_g solves (21) when $t = 0$. Also, let h_0 be the solution of (22) for $t = 0$, i.e., h_0 is the harmonic function with trace of vanishing mean on Γ, which satisfies the Neumann condition $\sigma_b \frac{\partial h_0}{\partial \mathbf{n}} = \frac{\epsilon_b}{\sigma_b} g$, in particular we have

$$h_0 = -\frac{\epsilon_b}{\sigma_b} \phi_g. \tag{24}$$

Next we use the estimates (19) in the forward problem to exhibit the t-asymptotic (with $t \to 0^+$) of the left-hand side of (13).

In all the estimates below the constant M may change from equation to equation, but at all times remains a constant dependent only on the domain Ω, the ellipticity constant $c > 0$, and, for brevity, on the constants σ_b and ϵ_b. Dependence on $r > 0$ in (5) will remain explicit.

By proposition 3.1 applied to (21) we obtain

$$\max\{\|v_t\|_1, \|\phi_g\|_1\} \leqslant M \|g\|_{-1/2}, \tag{25}$$

and when applied to (22) we obtain

$$\begin{aligned} \|h_t\|_1 &\leqslant M \left(\|\nabla \cdot \epsilon_t \nabla v_t\|_{-1} + \left\| \frac{\epsilon_t}{\sigma_t} \right\|_\infty \|g\|_{-1/2} \right) \\ &\leqslant M \|\epsilon_t\|_\infty (\|\nabla v_t\| + c\|g\|_{-1/2}) \\ &\leqslant M(\|v_t\|_1 + \|g\|_{-1/2}) \leqslant M\|g\|_{-1/2}, \end{aligned} \tag{26}$$

where the last inequality uses (25).

Now let

$$\delta v := v_t - \phi_g, \quad \text{and} \quad \delta h := h_t - h_0. \tag{27}$$

A simple calculation shows that (δv) solves

$$\begin{cases} \nabla \cdot \sigma_t \nabla (\delta v) = -t \nabla \cdot \tilde{\sigma} \nabla \phi_g, & \text{in} \quad \Omega, \\ \sigma_t \frac{\partial (\delta v)}{\partial \mathbf{n}} = t \tilde{\sigma} \frac{\partial \phi_g}{\partial \nu}, & \text{on} \quad \Gamma. \end{cases}$$

By proposition 3.1 we estimate

$$\begin{aligned}\|\delta v\|_1 &\leqslant tM\left(\|\nabla\cdot\tilde\sigma\nabla\phi_g\|_{-1}+\left\|\tilde\sigma\frac{\partial\phi_g}{\partial\nu}\right\|_{-1/2}\right)\\ &\leqslant tM\|\tilde\sigma\|_\infty(\|\nabla\phi_g\|+\|g\|_{-1/2})\\ &\leqslant tMr\|g\|_{-1/2},\end{aligned}\tag{28}$$

where the last inequality uses (5) and (25).

To estimate (δh) in (27), we note first that it solves

$$\begin{cases}\nabla\cdot\sigma_b\nabla(\delta h)=-\nabla\cdot(t\tilde\sigma\nabla h_t-\epsilon_t\nabla(\delta v)-t\tilde\epsilon\nabla\phi_g), & \text{in }\Omega\\ \sigma_b\frac{\partial(\delta h)}{\partial\mathbf{n}}=-t\frac{\tilde\sigma\epsilon_t}{\sigma_t^2}g+\left(\frac{\epsilon_t}{\sigma_t}-\frac{\epsilon_b}{\sigma_b}\right)g, & \text{on}\quad\Gamma.\end{cases}\tag{29}$$

Also, by using (7) and (5) we have

$$\left|\frac{\epsilon_t}{\sigma_t}-\frac{\epsilon_b}{\sigma_b}\right|=t\left|\frac{\sigma_b\tilde\epsilon-\epsilon_b\tilde\sigma}{\sigma_t\sigma_b}\right|\leqslant trc\left(1+\frac{\epsilon_b}{\sigma_b}\right).\tag{30}$$

By applying once more proposition 3.1 to (29) we estimate

$$\begin{aligned}\|\delta h\|_1 &\leqslant M\Bigg(t\|\tilde\sigma\|_\infty\|\nabla h_t\|+\|\epsilon_t\|_\infty\|\nabla(\delta v)\|+t\|\tilde\epsilon\|_\infty\|\nabla\phi_g\|\\ &\quad+\left\|\frac{\tilde\sigma\epsilon_t}{\sigma_t^2}\right\|_\infty\|g\|_{-1/2}+trc\left(1+\frac{\epsilon_b}{\sigma_b}\right)\|g\|_{-1/2}\Bigg)\\ &\leqslant tMr\|g\|_{-1/2},\end{aligned}\tag{31}$$

where in the last inequality we used in the estimates (26), (28), (25), and (30) in this order.

We have now all the ingredients necessary to establish (8). We start by multiplying the top equation of (22) by ϕ_f, and use Green's formula once to obtain

$$\int_\Gamma\sigma_t\frac{\partial h_t}{\partial\nu}\phi_f\,\mathrm{d}s-\int_\Omega\sigma_t\nabla h_t\nabla\phi_g=-\int_\Gamma\epsilon_t\frac{\partial v_t}{\partial\nu}\phi_f\,\mathrm{d}s+\int_\Omega\epsilon_t\nabla v_t\cdot\nabla\phi_f\,\mathrm{d}x.$$

Now use the Neumann condition in (22) and (21) to cancel the two boundary integrals above and obtain the key identity

$$\int_\Omega(\sigma_t\nabla h_t+\epsilon_t\nabla v_t)\cdot\nabla\phi_f\,\mathrm{d}x=0.\tag{32}$$

In the identity (32) we first replace $\sigma_t=\sigma_b+t\tilde\sigma$, $\epsilon_t=\epsilon_b+t\tilde\epsilon$, and separate the zero order terms to get

$$\int_\Omega(\sigma_b\nabla h_t+\epsilon_b\nabla v_t)\cdot\nabla\phi_f\,\mathrm{d}x=-t\int_\Omega(\tilde\sigma\nabla h_t+\tilde\epsilon\nabla v_t)\cdot\nabla\phi_f\,\mathrm{d}x.$$

Now use $h_t=h_0+(\delta h)$, and $v_t=\phi_g+(\delta v)$ and further separate the first order from the quadratic terms in the right-hand side above. Upon one division by $\epsilon_b\sigma_b$ we obtain

$$\int_\Omega\left(\frac{1}{\epsilon_b}\nabla h_t+\frac{1}{\sigma_b}\nabla v_t\right)\cdot\nabla\phi_f\,\mathrm{d}x=-\frac{t}{\epsilon_b\sigma_b}\int_\Omega(\tilde\sigma\nabla h_0+\tilde\epsilon\nabla\phi_g)\cdot\nabla\phi_f\,\mathrm{d}x-t^2r^2R(t),\tag{33}$$

where r is the bound in (5) and the remainder

$$R(t):=\frac{1}{tr^2\sigma_b\epsilon_b}\int_\Omega[\tilde\sigma\nabla(\delta h)+\tilde\epsilon\nabla(\delta v)]\cdot\nabla\phi_f\,\mathrm{d}x.\tag{34}$$

Using the $H^1(\Omega)$-estimates of (δv) in (28) and of (δh) in (31), it is easy to see the uniform bound

$$|R(t)|\leqslant M\|g\|_{-1/2}\|f\|_{-1/2},\tag{35}$$

for some constant M dependent only on Ω, c, σ_b and ϵ_b.

Returning to (33), we use Green's identity in the left-hand side, and the relation (24) between h_0 and ϕ_g to get

$$\int_\Gamma f\left(\frac{h_t}{\epsilon_b}+\frac{v_t}{\sigma_b}\right)\mathrm{d}s = t\int_\Omega\left(\frac{\tilde\sigma}{\sigma_b}-\frac{\tilde\epsilon}{\epsilon_b}\right)\nabla\phi_g\nabla\phi_f\,\mathrm{d}x - t^2r^2R(t). \tag{36}$$

Finally, corollary 2.2 in the formula (23) identifies the left-hand side in (36) to conclude the t-asymptotic expansion

$$\left\langle f,\ \frac{\mathrm{d}}{\mathrm{d}\omega}\bigg|_{\omega=0}\left(\frac{\omega}{\sigma_b}-\frac{\mathrm{i}}{\epsilon_b}\right)\mathcal{N}_{\gamma_\omega^t}g\right\rangle = t\int_\Omega[\delta Q]\nabla\phi_g\nabla\phi_f\,\mathrm{d}x - t^2r^2R(t). \tag{37}$$

This proves theorem 1.1.

4. A reconstruction method for δQ using the complete electrode model

Recall the notations in (4)

$$\sigma_t := \sigma_b + t\tilde\sigma, \quad \epsilon_t := \epsilon_b + t\tilde\epsilon, \quad \gamma_\omega^t := \sigma_t + \mathrm{i}\omega\epsilon_t,$$

for some known constants σ_b, ϵ_b, and unknown $\tilde\sigma, \tilde\epsilon \in L^\infty(\Omega)$ of compact support in Ω. We assume the *a priori* bound in (5) holds for some $r > 0$.

In this section we first propose a method based on theorem 1.1 to approximately reconstruct

$$t[\delta Q] = \left(\frac{t\tilde\epsilon}{\epsilon_b}-\frac{t\tilde\sigma}{\sigma_b}\right),$$

for t sufficiently small.

The method uses the complete electrode model [35] as follows. Let L electrodes $e_1, \ldots, e_L$ of corresponding impedance $\zeta_1, \ldots, \zeta_L$ be placed at the boundary Γ. In each experiment we use a pair of electrodes, say (e_l, e_j) to inject/extract a time harmonic current $I_{lj}\cos\omega t$. There are $L(L-1)$-many experiments as (l, j) ranges in $\{1, \ldots, L\} \times \{1, \ldots, L\}$ with $l \neq j$. The complete electrode model (if γ_ω^t were known) assumes the complex voltage potential u_ω^{lj} would distribute inside according to the problem

$$\begin{cases} \nabla\cdot\left(\gamma_\omega^t\nabla u_\omega^{lj}\right) = 0, & \text{in } \Omega,\\ \left(u_\omega^{lj}+\zeta_l\gamma_\omega^t\frac{\partial u_\omega^{lj}}{\partial\mathbf{n}}\right)\Big|_{e_l} \equiv \text{const.} \equiv -\left(u_\omega^{lj}+\zeta_j\gamma_\omega^t\frac{\partial u_\omega^{lj}}{\partial\mathbf{n}}\right)\Big|_{e_j}\\ -\int_{e_l}\gamma_\omega^t\frac{\partial u_\omega^{lj}}{\partial\mathbf{n}}\,\mathrm{d}s = \int_{e_j}\gamma_\omega^t\frac{\partial u_\omega^{lj}}{\partial\mathbf{n}}\,\mathrm{d}s = I_{lj}\\ -\gamma_\omega^t\frac{\partial u_\omega^{lj}}{\partial\mathbf{n}} = 0, & \text{on } \Gamma\setminus\{e_j\cup e_l\}. \end{cases} \tag{38}$$

The voltage potential u_ω^{lj} also solves the Neumann problem (1) with the Neumann boundary data given by

$$g_{lj} := -\gamma_\omega^t\left.\frac{\partial u_\omega^{lj}}{\partial\mathbf{n}}\right|_\Gamma. \tag{39}$$

We note here that point-wise values of g_{lj} are unknown on the electrodes e_l, e_j.

At each electrode e_k not used in injection we measure $U_{\omega,k}^{lj}$, which gives

$$\int_{e_k} u_\omega^{lj}\,\mathrm{d}s = U_{\omega,k}^{lj}, \quad k \neq l, j. \tag{40}$$

At the electrode e_l where we 'inject' we may measure $U^{lj}_{\omega,l}$, which yields

$$\int_{e_l} u^{lj}_{\omega}\,\mathrm{d}s = U^{lj}_{\omega,l} + \zeta_l I_{lj}. \tag{41}$$

Similarly at the electrode e_j where we 'extract' we may measure $U^{lj}_{\omega,j}$, which yields

$$\int_{e_j} u^{lj}_{\omega}\,\mathrm{d}s = U^{lj}_{\omega,j} - \zeta_j I_{lj}. \tag{42}$$

Now theorem 2.1 yields the asymptotic

$$u^{lj} = v^{lj}_0 + \mathrm{i}\omega h^{lj}_1 + O(\omega^2).$$

By taking the real part and integrating over e_k in (15), and using the measured data in (40) we obtain

$$\int_{e_k}\left(\frac{v^{lj}_0}{\sigma_b} + \frac{h^{lj}_1}{\epsilon_b}\right)\mathrm{d}s = \Re\left\{\left(\frac{1}{\sigma_b} - \frac{\mathrm{i}}{\epsilon_b\omega}\right)\left(U^{lj}_{\omega,k} + \delta^{lj}_k\zeta_k I_{lj}\right)\right\} + O(\omega), \tag{43}$$

where

$$\delta^{lj}_k = \begin{cases} 1, & \text{if } k = l,\\ -1, & \text{if } k = j,\\ 0, & \text{if } k \neq l,\ j. \end{cases} \tag{44}$$

By using the t-asymptotic in (36) we obtain for an arbitrary $f \in H^{-1/2}(\Gamma)$ that

$$\int_\Omega t[\delta Q]\nabla\phi_{g_{lj}}\nabla\phi_f\,\mathrm{d}x = \int_\Gamma\left(\frac{v^{lj}_0}{\sigma_b} + \frac{h^{lj}_1}{\epsilon_b}\right)f\,\mathrm{d}s + t^2r^2R(t), \tag{45}$$

where $\phi_{g_{lj}}$, ϕ_f are the harmonic functions with traces of vanishing mean on Γ that satisfy the Neumann conditions

$$-\sigma_b\frac{\partial\phi_{g_lj}}{\partial\mathbf{n}} = g_{lj}, \quad -\sigma_b\frac{\partial\phi_f}{\partial\mathbf{n}} = f.$$

Recall that g_{lj} is not known point-wise on the electrodes e_l and e_j. We use instead an approximate ϕ_{lj} solution to

$$\begin{cases} \Delta\phi_{g_{lj}} = 0, & \text{in } \Omega,\\ -\sigma_b\frac{\partial\phi_{g_lj}}{\partial\mathbf{n}} = \frac{1}{|e_l|}I_{lj}, & \text{on } e_l,\\ -\sigma_b\frac{\partial\phi_{g_lj}}{\partial\mathbf{n}}\,\mathrm{d}s = -\frac{1}{|e_j|}I_{lj}, & \text{on } e_j\\ -\sigma_b\frac{\partial\phi_{g_{lj}}}{\partial\mathbf{n}} = 0, & \text{on } \Gamma\setminus(e_l\cup e_j). \end{cases} \tag{46}$$

Note that the choice of $f \in H^{-1/2}(\Gamma)$ is totally free. We choose f supported on the electrodes and constant on each electrode. For an arbitrary $\alpha = (\alpha_1,\ldots,\alpha_L) \in \mathbb{R}^L$, with $\alpha_1 + \alpha_2 + \cdots + \alpha_L = 0$, let

$$f_\alpha = \sum_{k=1}^{L}\alpha_k\chi_{e_k}, \tag{47}$$

where χ_{e_k} denotes the characteristic function of e_k.

By using (43) into (45) we obtain the system of equations

$$\int_\Omega t[\delta Q]\nabla\phi_{g_{lj}}\nabla\phi_{f_\alpha}\,\mathrm{d}x = \sum_{k=1}^{L}\alpha_k\Re\left\{\left(\frac{1}{\sigma_b} - \frac{\mathrm{i}}{\epsilon_b\omega}\right)\left(U^{lj}_{\omega,k} + \delta^{lj}_k\zeta_k I_{lj}\right)\right\} + t^2r^2R(t) + \omega\tilde{R}(\omega), \tag{48}$$

where δ_k^{lj} is given by (44). Moreover, according to (35), we have the error estimate

$$|R(t)| \leqslant M\|g_{lj}\|_{-1/2}\|f\|_{-1/2},$$

(M depends only on Ω, c, σ_b, and ϵ_b), and following from (16),

$$|\tilde{R}(\omega)| \leqslant N \left\| \frac{\epsilon}{\sigma} \right\|_\infty^2 \left(1 - \left\| \frac{\epsilon\omega}{\sigma} \right\|_\infty\right)^{-1} \|g_{lj}\|_{-1/2}\|f\|_{-1/2}, \tag{49}$$

for some constant N which depends on c only.

For t and ω sufficiently small we use the linear approximation

$$\int_\Omega t[\delta Q]\nabla\phi_{g_{lj}}\nabla\phi_{f_\alpha}\,\mathrm{d}x \approx \sum_{k=1}^{L} \alpha_k \Re\left\{\left(\frac{1}{\sigma_b} - \frac{\mathrm{i}}{\epsilon_b\omega}\right)\left(U_{\omega,k}^{lj} + \delta_k^{lj}\zeta_k I_{lj}\right)\right\}. \tag{50}$$

In the numerical method below we assume that both $\tilde{\sigma}$ and $\tilde{\epsilon}$, and hence δQ are piecewise constant. Let $\Omega = \cup_{p=1}^N \Omega_p$ be a partition of the imaging domain, for some arbitrarily fixed N. If χ_{Ω_p} denotes the characteristic function of Ω_p, then

$$t\tilde{\sigma} = \sum_{p=1}^{N} x_p\chi_{\Omega_p}, \quad t\tilde{\epsilon} = \sum_{p=1}^{N} y_p\chi_{\Omega_p}, \quad t[\delta Q] = \sum_{p=1}^{N} z_p\chi_{\Omega_p},$$

for some unknowns $x_1, \ldots x_N$, $y_1, \ldots, y_N$, and $z_1, \ldots, z_L$ related by

$$z_k = \left(\frac{x_k}{\sigma_b} - \frac{y_k}{\epsilon_b}\right), \quad k = 1, \ldots, N. \tag{51}$$

We first use (50) to determine $z_1, \ldots, z_N$ by solving the linear system

$$\sum_{p=1}^{N} z_p \int_{\Omega_p} \nabla\phi_{g_{lj}}\nabla\phi_{f_\alpha}\,\mathrm{d}x \approx \sum_{k=1}^{L} \alpha_k \Re\left\{\left(\frac{1}{\sigma_b} - \frac{\mathrm{i}}{\epsilon_b\omega}\right)\left(U_{\omega,k}^{lj} + \delta_k^{lj}\zeta_k I_{lj}\right)\right\} \tag{52}$$

for $l, j \in \{1, \ldots, L\}$ with $l \neq j$ and sufficiently many choices of f_α as in (47).

5. Separate reconstruction of small perturbations in conductivity and permittivity

In this section we adapt the original arguments of Calderón to recover an approximate $t\tilde{\sigma}$ from boundary information of the real part $\Re(u_\omega)$ of the voltage potential for t sufficiently small. In combination with the independent reconstruction of $\left(\frac{t\tilde{\sigma}}{\sigma_b} - \frac{t\tilde{\epsilon}}{\epsilon_b}\right)$ in section 4 above we can then recover $t\tilde{\epsilon}$.

For $g, f \in H^{-1/2}(\Gamma)$ real valued, recall that ϕ_g, ϕ_f denote the harmonic maps (with mean vanishing trace on Γ) which satisfy the Neumann conditions $-\sigma_b\frac{\partial\phi_g}{\partial\nu} = g$, respectively $-\sigma_b\frac{\partial\phi_f}{\partial\nu} = f$. Let also v_t be the solution of the problem (21).

The analytic expansion in theorem 2.1 shows that

$$\Re(u_\omega) = v_t + \omega^2 R_1(\omega),$$

where

$$|R_1(\omega)| \leqslant N \left\| \frac{\epsilon}{\sigma} \right\|_\infty^2 \left(1 - \left\| \frac{\epsilon\omega}{\sigma} \right\|_\infty^2\right)^{-1} \|g\|_{-1/2}, \tag{53}$$

for some constant N which depends only on the domain Ω, and the ellipticity constant $c > 0$.

By multiplying the top equation in (21) by ϕ_f, and using $\delta v := v_t - \phi_g$ as before, Green's formula yields

$$\int_\Omega (t\tilde{\sigma})\nabla\phi_g \cdot \nabla\phi_f\,\mathrm{d}x = \int_\Gamma (fv_t - g\phi_f)\,\mathrm{d}s + R_2(t), \tag{54}$$

where the remainder term

$$R_2(t) := \int_\Omega t\tilde{\sigma}\nabla(\delta v)\cdot\nabla\phi_f \,\mathrm{d}x.$$

The estimate $\|\phi_f\|_1 \leqslant C\|f\|_{1/2}$ together with (28) yields the error estimate

$$|R_2(t)| \leqslant t^2 r^2 M\|g\|_{-1/2}\|f\|_{-1/2}. \tag{55}$$

Note that the first term in the right-hand side of (54) is known. By ignoring the remainder term in the right-hand side of (54) we recover an approximate perturbation $t\tilde{\sigma}$ as follows.

For some arbitrarily fixed integer N recall the partition $\Omega = \cup_{p=1}^N \Omega_p$, the characteristic function χ_{Ω_p} of Ω_p, and the piecewise constant representation

$$t\tilde{\sigma} = \sum_{p=1}^N x_p \chi_{\Omega_p}$$

for some unknown $x_1, \ldots, x_N$.

From (54) with $g = g_{lj}$ supported on $e_k \cup e_j$ and $f = f_\alpha$, $\alpha = (\alpha_1, \ldots., \alpha_L) \in \mathbb{R}^L$ with $\alpha_1 + \alpha_2 + \cdots + \alpha_L = 0$ as in (47), we obtain the linear system

$$\begin{aligned}\sum_{p=1}^N x_p \int_{\Omega_p} \nabla\phi_{g_{lj}}\nabla\phi_{f_\alpha}\,\mathrm{d}x &\approx \sum_{k=1}^L \left(\alpha_k \Re\left\{U^{lj}_{\omega,k} + \delta^{lj}_k \zeta_k I_{lj}\right\} - \int_{e_k} g_{lj}\phi_\alpha \,\mathrm{d}s\right)\\ &= \sum_{k=1}^L \alpha_k \Re\left\{U^{lj}_{\omega,k} + \delta^{lj}_k \zeta_k I_{lj}\right\} - \int_{e_l\cup e_j} g_{lj}\phi_{f_\alpha}\,\mathrm{d}s,\end{aligned} \tag{56}$$

where the coefficients δ^{lj}_k are defined in (44).

Since we work with the complete electrode model, the values of the injected current g_{lj} are not known point-wise, instead we further approximate the last term in the right-hand side above by assuming a piecewise constant current on the electrodes. The values $x_1, \ldots, x_N$ are thus obtained as solutions of the linear system

$$\sum_{p=1}^N x_p \int_{\Omega_p} \nabla\phi_{g_{lj}}\nabla\phi_{f_\alpha}\,\mathrm{d}x \approx \sum_{k=1}^L \alpha_k \Re\left\{U^{lj}_{\omega,k} + \delta^{lj}_k \zeta_k I_{lj}\right\} - I_{lj}\left(|e_l|\int_{e_l}\phi_{f_\alpha}\,\mathrm{d}s - |e_j|\int_{e_j}\phi_{f_\alpha}\,\mathrm{d}s\right) \tag{57}$$

for $l, j \in \{1, \ldots, L\}$ with $l \neq j$ and sufficiently many choices of f_αs as in (47).

Finally, from (51) the values of permittivity are obtained by

$$y_k = \epsilon_b\left(\frac{x_k}{\sigma_b} - z_k\right), \quad k = 1, \ldots, N. \tag{58}$$

Note that N establishes an *a priori* resolution on our image. Then how large can it be? In principle N can be arbitrarily large. While there can be at most $L(L-1)$ combinations to yield $\phi_{g_{lj}}$, the parameter α which fixes ϕ_{f_α} ranges in an $(L-1)$ dimension subspace of $\mathbb{R}^L$. However, we should note that the error bound in (45) depends on the $H^{-1/2}(\Gamma)$-norm of f. In particular, even if t were small, the linearization error we made for large $\|\alpha\|$ may be large. Also, (49) shows that the linearization error may grow as frequency ω approaches the critical value $1/\|\epsilon/\sigma\|_\infty$.

We also note that the choice of (l, j) being independent of α has a practical application. It is difficult to measure the voltage at the electrodes where current is injected at the same time. Then for a fixed pair (e_l, e_j) choose an α with $\alpha_l = \alpha_j = 0$. In this case the right-hand side of (52) does not depend on the knowledge of the induced voltage on the electrodes e_l, and e_j used for injection, i.e. formulas (42) and (41) are not used in the reconstruction.

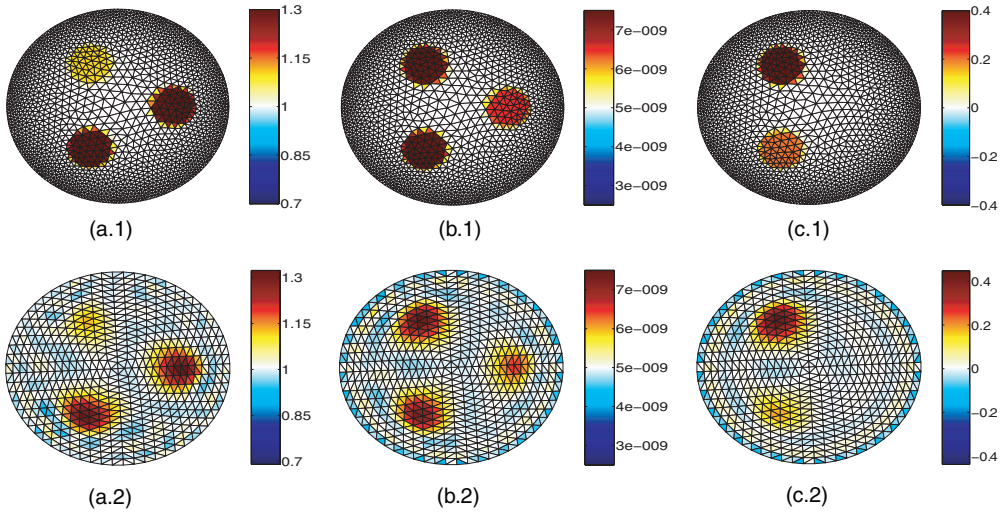

Figure 1. Symmetric case. Figures on the top row are true images of the conductivity σ_t in (a.1), the absolute permittivity ε_t in (b.1), respectively of $t[\delta Q]$ in (c.1). Figures on the bottom row are reconstructed images of σ_t in (a.2), of ε_t in (b.2), respectively of $t[\delta Q]$ in (c.2) based on the proposed linearization method. The reconstruction in (c.2) is independent of the one in (a.2). We used 5% random noise in the data.

6. Numerical simulation

To show the feasibility of the linearization method proposed in the previous sections, we performed two numerical experiments at an angular frequency $\nu = 2\pi \times 10^3$ Hz.

The numerical experiments are presented in absolute values for the permittivity (not relative to the air). The domain Ω is the unit disc. We assume a homogeneous background conductivity $\sigma_b = 1$ and absolute permittivity $\varepsilon_b = 0.5 \times 10^{-8}$. A number of $L = 32$ electrodes of equal length $\pi/48$ are equally spaced around the circumference.

For the first simulation, we assume that embedded in Ω there are three disc anomalies D_k with radii 0.2, and centers located at $0.5\left\langle \cos\left((k-1)\frac{2\pi}{3}\right), \sin\left((k-1)\frac{2\pi}{3}\right)\right\rangle$, for $k = 1, 2, 3$. It was assumed that the background admittivity $\sigma_b + \mathrm{i}\omega\epsilon_b$ was perturbed by

$$t(\tilde{\sigma} + \mathrm{i}\nu\tilde{\varepsilon}) = \begin{cases} \frac{3\sigma_b}{10} + \mathrm{i}\nu\frac{3\varepsilon_b}{10}, & \text{in } D_1, \\ \frac{\sigma_b}{10} + \mathrm{i}\nu\frac{\varepsilon_b}{2}, & \text{in } D_2, \\ \frac{3\sigma_b}{10} + \mathrm{i}\nu\frac{\varepsilon_b}{2}, & \text{in } D_3. \\ 0, & \text{otherwise;} \end{cases} \tag{59}$$

see figures 1(a.1) and (b.1) which show images of the simulated conductivity $\sigma_t = \sigma_b + t\tilde{\sigma}$, respectively of the permittivity $\varepsilon_t = \varepsilon_b + t\tilde{\varepsilon}$, to be recovered. Note that the admittivity $\sigma_t + \mathrm{i}\nu\varepsilon_t$ satisfies the condition (9) whenever ν is less than 10 kHz.

In order to obtain the forward solutions, we solved the complete electrode model (38) (recall that the change of scale does not change the admittivity) via the finite element method with 3215 triangular elements and 1704 nodes. For the electrode impedance, we assumed that $\zeta_k = 0.01$, $k = 1, 2, \ldots, L$. We performed 32 forward experiments for adjacent pairs of electrodes (e_l, e_j), with $j = l + 1 \pmod{32}$, $l \in \{1, \ldots, 32\}$. This allowed for a reconstruction mesh of $N = 32 \times 32 = 2014$ elements.

To introduce noise in the simulated data $U_\omega^{lj} = (U_{\omega,1}^{lj}, U_{\omega,2}^{lj}, \ldots, U_{\omega,L}^{lj}) \in \mathbb{C}^L$ in (40) we computed the solution ψ_ω^{lj} to (38) at the background admittivity, and let

$$\Psi_\omega^{lj} = \left(\int_{e_1} \psi_\omega^{lj} \, \mathrm{d}s, \int_{e_2} \psi_\omega^{lj} \, \mathrm{d}s, \ldots, \int_{e_L} \psi_\omega^{lj} \, \mathrm{d}s \right) \in \mathbb{C}^L.$$

For reconstruction, we added the nos_lev $= 5\%$ random noise to the forward simulated data by the formulas

$$\Re(U_\omega^{lj}) + (\text{nos\_lev}) * \sqrt{\frac{\left[\Re\left(U_\omega^{lj} - \Psi_\omega^{lj}\right)\right]^2}{M}} * (\text{rand\_num}),$$

$$\Im(U_\omega^{lj}) + (\text{nos\_lev}) * \sqrt{\frac{\left[\Im\left(U_\omega^{lj} - \Psi_\omega^{lj}\right)\right]^2}{M}} * (\text{rand\_num}),$$

where rand_num is a vector of random numbers distributed in $(-1, 1)$.

Using the fdEIT/ data the goal is to reconstruct the quantity

$$t[\delta Q] = t\left(\frac{\tilde{\varepsilon}}{\varepsilon_b} - \frac{\tilde{\sigma}}{\sigma_b}\right) = \begin{cases} 0 & \text{in } D_1, \\ 0.4 & \text{in } D_2, \\ 0.2 & \text{in } D_3 \\ 0 & \text{otherwise} \end{cases} \tag{60}$$

shown in figure 1(c.1); note that the scaling in permittivity leaves $t\delta Q$ invariant.

In the reconstruction we used the same configuration of electrodes to generate the harmonic functions $\phi_{g_{lj}}$, and ϕ_{f_α}, i.e. α's were of the type $\langle 0, \ldots, 1, -1, 0, \ldots \rangle$. The reconstruction is based on solving the $N \times N$ linear system (52) with $N = 32 \times 32 = 2014$. The sensitivity matrix in (52) was computed by using the corresponding forward solutions in the absence of the anomaly. No regularization was used for inverting the matrix.

Figure 1(c.2) shows the reconstructed image of the $t[\delta Q]$ by solving the linear system in (52). The interesting part in this reconstruction is that the fdEIT data is blind to the presence of the anomaly D_1, as forecast theoretically.

Next we use the method in section 5 to separately reconstruct conductivity and permittivity by also employing (single frequency) EIT data encoded in the real part of the voltage potential. Figure 1(a.2) shows the reconstruction of conductivity $\sigma_t = \sigma_b + t\tilde{\sigma}$, with $t\tilde{\sigma}$ obtained via solving the linear system (57). In combination with the reconstruction of $t[\delta Q]$ we are also able to recover $t\tilde{\varepsilon}$ via (58), and thus the permittivity $\varepsilon_t = \varepsilon_b + t\tilde{\varepsilon}$ shown in figure 1(b.2).

In the second experiment we carried out a simulation in which four anomalies (two discs and two ellipses) were located non-symmetrically across the unit disc Ω. Let us denote by D_1, D_2, D_3, D_4, respectively, the bigger disc near the center, the smaller disc, the horizonal ellipse, the vertical ellipse in the figure 2(a.1). Then we assumed that the background admittivity was perturbed by

$$t(\tilde{\sigma} + \mathrm{i}\nu\tilde{\varepsilon}) = \begin{cases} \frac{2\sigma_b}{10} + \mathrm{i}\nu\frac{7\varepsilon_b}{10}, & \text{in } D_1, \\ \frac{3\sigma_b}{10} + \mathrm{i}\nu\frac{3\varepsilon_b}{10}, & \text{in } D_2, \\ \frac{3\sigma_b}{10} + \mathrm{i}\nu\frac{3\varepsilon_b}{10}, & \text{in } D_3. \\ \frac{\sigma_b}{10} + \mathrm{i}\nu\frac{\varepsilon_b}{2}, & \text{in } D_4. \\ 0, & \text{otherwise.} \end{cases} \tag{61}$$

In particular, the smaller disc D_2 on the right and the horizontal ellipse D_3 on the top have the zero value of $t[\delta Q]$, and they cannot be identified solely from the fdEIT data, see figure 2(c.2).

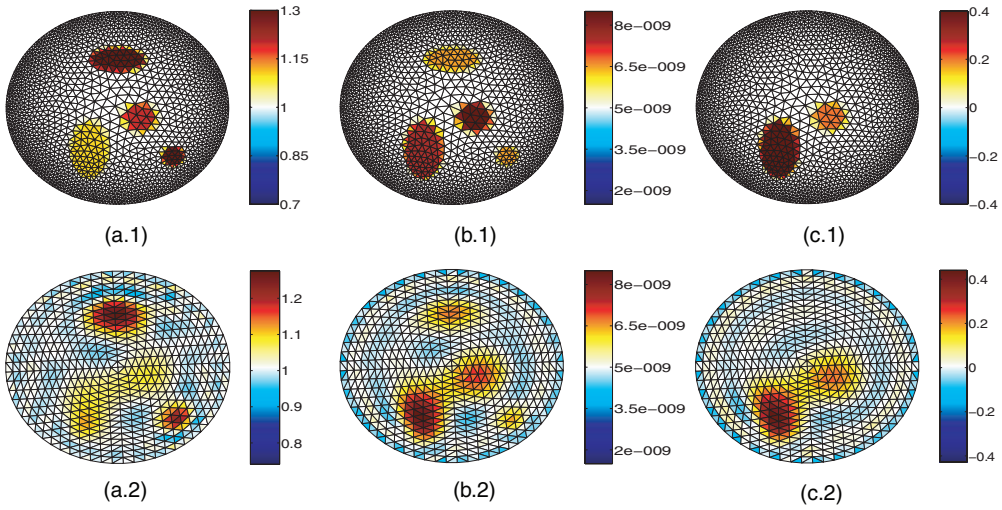

Figure 2. Non-symmetric case. Figures on the top row are true images of the conductivity σ_t in (a.1), the absolute permittivity ε_t in (b.1), respectively of $t[\delta Q]$ in (c.1). Figures on the bottom row are reconstructed images of σ_t in (a.2), of ε_t in (b.2), respectively of $t[\delta Q]$ in (c.2) based on the proposed linearization method. The reconstruction in (c.2) is independent of the one in (a.2). We used 5% random noise in the data.

7. Conclusions

We present a method to recover small perturbations from constants in the electrical conductivity $\delta\sigma$ and relative (to the air's) permittivity $\delta\epsilon$ of a body from boundary measurements at low frequencies.

The method is based on the asymptotic expansion of the frequency differential of the Neumann-to-Dirichlet map with respect to both frequency and perturbation size. Errors due to neglecting small asymptotic terms are estimated in terms of the coercivity constant, the domain, and *a priori* estimates of the perturbations.

From the main asymptotic terms we show that the frequency differential of an appropriately scaled Neumann-to-Dirichlet map recovers $\frac{\delta\epsilon}{\epsilon_b} - \frac{\delta\sigma}{\sigma_b}$. In particular, from frequency differential data alone, one will not be able to distinguish subregions where the relative perturbation in conductivity equates the relative perturbation in permittivity. If, in addition, we also take into account the real part of the induced voltage potential, both perturbations $\delta\sigma$ and $\delta\epsilon$ can be determined separately.

We propose a numerical scheme based on finitely many electrode configuration, and show its feasibility in two numerical experiments. In the simulations the domain contains subregions in which the relative perturbation in conductivity is the same as the relative perturbation in permittivity. These subregions cannot be distinguished from the background when using the frequency differential data alone, as explained theoretically. However, when the real part of the voltage potential at the boundary is also employed, these subregions are recovered.

Acknowledgments

The authors would like to thank the anonymous referees for their constructive criticism on an earlier version. The first author would like to thank Hanbat National University for the

financial support which made his sabbatical visit to A Tamasan at the University of Central Florida possible. The work of the second author was supported by NSF grant DMS 1312883.

Appendix. Proof of theorem 2.1

We first establish a basic estimate for the double series of functions satisfying the recurrence (12).

Lemma A.1. *Let* $\{v_{2k}\}$ *and* $\{h_{2k-1}\}$ *be defined recursively in (12). Then*

$$\left[\int_\Omega \sigma|\nabla h_{2k-1}|^2\,\mathrm{d}x\right]^{\frac{1}{2}} \leqslant \left\|\frac{\epsilon}{\sigma}\right\|_\infty^{2k-1}\left[\int_\Omega \sigma|\nabla v_0|^2\,\mathrm{d}x\right]^{\frac{1}{2}}, \quad \textit{and} \tag{A.1}$$

$$\left[\int_\Omega \sigma|\nabla v_{2k}|^2\,\mathrm{d}x\right]^{\frac{1}{2}} \leqslant \left\|\frac{\epsilon}{\sigma}\right\|_\infty^{2k}\left[\int_\Omega \sigma|\nabla v_0|^2\,\mathrm{d}x\right]^{\frac{1}{2}}, \quad k=1,2,\ldots. \tag{A.2}$$

Proof. Fix an index k. From the divergence theorem we have that

$$\begin{aligned}
\int_\Omega \sigma|\nabla h_{2k-1}|^2\,\mathrm{d}x &= \int_\Gamma \sigma\frac{\partial h_{2k-1}}{\nu}h_{2k-1}\,\mathrm{d}s - \int_\Omega \nabla\cdot(\sigma\nabla h_{2k-1})h_{2k-1}\,\mathrm{d}x\\
&= (-1)^{k-1}\int_\Gamma\left(\frac{\epsilon}{\sigma}\right)^{2k-1} g h_{2k-1}\,\mathrm{d}s + \int_\Omega \nabla\cdot(\epsilon\nabla v_{2k-2})h_{2k-1}\,\mathrm{d}x\\
&= (-1)^{k-1}\int_\Gamma\left(\frac{\epsilon}{\sigma}\right)^{2k-1} g h_{2k-1}\,\mathrm{d}s + \int_\Gamma \epsilon\frac{\partial v_{2k-2}}{\partial\nu}h_{2k-1}\,\mathrm{d}s\\
&\quad - \int_\Omega \epsilon\nabla v_{2k-2}\cdot\nabla h_{2k-1}\,\mathrm{d}x\\
&= (-1)^{k-1}\int_\Gamma\left(\frac{\epsilon}{\sigma}\right)^{2k-1} g h_{2k-1}\,\mathrm{d}s + (-1)^k\int_\Gamma\frac{\epsilon}{\sigma}\left(\frac{\epsilon}{\sigma}\right)^{2k-2} g h_{2k-1}\,\mathrm{d}s\\
&\quad - \int_\Omega \epsilon\nabla v_{2k-2}\cdot\nabla h_{2k-1}\,\mathrm{d}x = -\int_\Omega \epsilon\nabla v_{2k-2}\cdot\nabla h_{2k-1}\,\mathrm{d}x,
\end{aligned}$$

where in the second equality we use the top equation as well as the Neumann boundary conditions in (12).

By applying Cauchy's inequality to the right-hand side above we obtain

$$\int_\Omega \sigma|\nabla h_{2k-1}|^2\,\mathrm{d}x \leqslant \left\|\frac{\epsilon}{\sigma}\right\|_\infty\left[\int_\Omega \sigma|\nabla v_{2k-2}|^2\,\mathrm{d}x\right]^{\frac{1}{2}}\left[\int_\Omega \sigma|\nabla h_{2k-1}|^2\,\mathrm{d}x\right]^{\frac{1}{2}},$$

and thus

$$\left[\int_\Omega \sigma|\nabla h_{2k-1}|^2\,\mathrm{d}x\right]^{\frac{1}{2}} \leqslant \left\|\frac{\epsilon}{\sigma}\right\|_\infty\left[\int_\Omega \sigma|\nabla v_{2k-2}|^2\,\mathrm{d}x\right]^{\frac{1}{2}}. \tag{A.3}$$

Similarly we obtain

$$\left[\int_\Omega \sigma|\nabla v_{2k}|^2\,\mathrm{d}x\right]^{\frac{1}{2}} \leqslant \left\|\frac{\epsilon}{\sigma}\right\|_\infty\left[\int_\Omega \sigma|\nabla h_{2k-1}|^2\,\mathrm{d}x\right]^{\frac{1}{2}}. \tag{A.4}$$

By induction, the estimates (A.2) and (A.1) follow. □

Proof of theorem 2.1. Upon identifying the real and the imaginary part, The Neumann problem (1) is equivalent to the following elliptic system:

$$\begin{cases} \nabla\cdot(\sigma\nabla v_\omega) = \omega\nabla\cdot(\epsilon\nabla h_\omega) & \text{in} \quad \Omega, \\ \nabla\cdot(\sigma\nabla h_\omega) = -\omega\nabla\cdot(\epsilon\nabla v_\omega) & \text{in} \quad \Omega, \\ -(\sigma^2+\omega^2\epsilon^2)\frac{\partial v_\omega}{\partial \mathbf{n}} = \sigma g, \quad \text{on} \quad \Gamma, \\ -(\sigma^2+\omega^2\epsilon^2)\frac{\partial h_\omega}{\partial \mathbf{n}} = -\omega\epsilon g, \quad \text{on} \quad \Gamma, \\ \int_\Gamma v_\omega\,\mathrm{d}s = \int_\Gamma h_\omega\,\mathrm{d}s = 0. \end{cases} \tag{A.5}$$

□

We seek solutions in the ansatz

$$v(x,\omega) := \sum_{k=0}^{\infty} v_{2k}(x)\omega^{2k}, \quad \text{and} \quad h(x,\omega) := \sum_{k=1}^{\infty} h_{2k-1}(x)\omega^{2k-1}. \tag{A.6}$$

Let us assume first that the series representation in (A.6) are convergent in $H^1(\Omega)$. If (A.5) is satisfied, then

$$\nabla\cdot(\sigma\nabla v_0) + \sum_{k=1}^{\infty}\nabla\cdot(\sigma\nabla v_{2k} - \epsilon\nabla h_{2k-1})\omega^{2k} = 0, \quad \text{and}$$
$$\sum_{k=0}^{\infty}\nabla\cdot(\sigma\nabla h_{2k+1} + \epsilon\nabla v_{2k})\omega^{2k+1} = 0,$$

where the divergence is taken in the weak sense. In particular we obtain the top equation in (11) and top two equations in (12).

By our assumption, both series are convergent in $H^1(\Omega)$, and therefore $\frac{\partial v_\omega}{\partial \mathbf{n}}$, and $\frac{\partial h_\omega}{\partial \mathbf{n}}$ have well defined trace in $H^{-1/2}(\Gamma)$, which are the corresponding sum of the traces of the terms. Moreover, since the traces of v_ω and h_ω are the sum (in $H^{1/2}(\Gamma)$) of the series of the traces of v_{2k}, and h_{2k+1}, $k = 0, 1, \ldots$, the zero mean condition will be also satisfied for each term v_{2k}, and h_{2k+1}.

We are left to check the Neumann conditions in (12). Starting from the Neumann condition for v_ω in (A.5) we get

$$(-\sigma^2+\omega^2\epsilon^2)\sum_{k=0}^{\infty}\frac{\partial v_{2k}}{\partial \mathbf{n}}\omega^{2k} = \sigma g.$$

Upon identifying like terms, it is easy to see that

$$-\sigma\frac{\partial v_0}{\partial \mathbf{n}} = g, \quad \text{and} \quad -\sigma^2\frac{\partial v_{2k}}{\partial \mathbf{n}} = \epsilon^2\frac{\partial v_{2k-2}}{\partial \mathbf{n}}.$$

By induction in the second equality above we obtain the Neumann condition for v_{2k} in (12). A similar calculation starting from the Neumann condition for h_ω in (A.5), yields the Neumann condition for h_{2k-1} in (12), $k = 1, 2, \ldots$.

Conversely, for $g \in H^{-1/2}(\Gamma)$ let v_0 be the solution of (11) and define two sequences of functions $\{v_k\}_0^\infty$ and $\{h_k\}_1^\infty$ via the recurrence (12). We denote by $\|\cdot\|$ the $L^2(\Omega)$-norm. From (A.2) it follows that for any $k = 1, 2, \ldots$,

$$\begin{aligned} \|\nabla v_{2k}\|\omega^{2k} &\leqslant \sqrt{c}\left[\int_\Omega \sigma|\nabla v_{2k}|^2\,\mathrm{d}x\right]^{\frac{1}{2}}\omega^{2k} \\ &\leqslant \sqrt{c}\left\|\frac{\omega\epsilon}{\sigma}\right\|_\infty^{2k}\left[\int_\Omega \sigma|\nabla v_0|^2\,\mathrm{d}x\right]^{\frac{1}{2}} \leqslant c\|\nabla v_0\|\left\|\frac{\omega\epsilon}{\sigma}\right\|_\infty^{2k}, \end{aligned} \tag{A.7}$$

and, similarly,

$$\|\nabla h_{2k-1}\|\omega^{2k-1} \leqslant c\|\nabla v_0\|\left\|\frac{\omega\epsilon}{\sigma}\right\|_\infty^{2k-1}. \tag{A.8}$$

Now consider the series (A.6) to formally define some $v(x,\omega)$ and $h(x,\omega)$. We show next that the series converge in $H^1(\Omega)$ and that they satisfy the boundary conditions in (A.5). Indeed, since ω satisfies the frequency range condition $\left\|\frac{\omega\epsilon}{\sigma}\right\|_\infty < 1$, the $L^2(\Omega)$-convergence of the series of gradients is guaranteed from (A.7) and (A.8) to well define $\nabla_x v(x,\omega)$ and $\nabla_x h(x,\omega)$ in $L^2(\Omega)$.

Now using the Neumann conditions in (12), and again the frequency range condition (9), we get the $H^{-1/2}$-summability of the series

$$\sum_{k=0}^{\infty}\omega^{2k}\frac{\partial v_{2k}}{\partial \nu} = -\frac{g}{\sigma}\sum_{k=0}^{\infty}\left(-\frac{\omega^2\epsilon^2}{\sigma^2}\right)^k = -\frac{\sigma g}{\sigma^2+\omega^2\epsilon^2}. \tag{A.9}$$

Upon multiplication of (A.9) by arbitrary functions in $H^{1/2}(\Gamma)$, integrating over Γ and applying Green's formula, the duality between $H^{-1/2}(\Gamma)$ and $H^{1/2}(\Gamma)$ then shows $H^{1/2}(\Gamma)$-summability in the series of the traces

$$\sum_{k=0}^{\infty}\omega^{2k}\ v_{2k}|_\Gamma\,.$$

In particular this will carry the zero mean property from each term to the sum.

With the L^2-summability for the gradient shown previously, we conclude the summability of the $H^1(\Omega)$-sense. Moreover, the calculation (A.9) showed that

$$-(\sigma^2+\omega^2\epsilon^2)\frac{\partial v(\cdot,\omega)}{\partial \mathbf{n}} = \sigma g, \quad \text{on} \quad \Gamma,$$

which is the Neumann condition for v_ω in (A.5).

A similar geometric summation as in (A.9), and the duality argument above shows that the series defining $h(\cdot,\omega)$ is also summable in $H^1(\Omega)$ and that $h(\cdot,\omega)$ satisfies the Neumann condition for h_ω in (A.5).

References

[1] Astala K and Päivärinta L 2006 Calderón's inverse conductivity problem in the plane *Ann. Math.* **163** 265–99

[2] Bayford R H 2006 Bioimpedance tomography (electrical impedance tomography) *Annu. Rev. Biomed. Eng.* **8** 63–91

[3] Beals R and Coifman R R 1985 Multidimensional inverse scatterings and nonlinear partial differential equations *Pseudodifferential Operators and Applications (Proceedings of Symposia in Pure Mathematics* vol 43*)* (Providence, RI: American Mathematical Society)

[4] Borcea L 2002 Electrical impedance tomography *Inverse Problems* **18** R99–136

[5] Brown B H, Barber D C, Morice A H, Leathard A and Sinton A 1994 Cardiac and respiratory related electrical impedance changes in the human thorax *IEEE Trans. Biomed. Eng.* **41** 729–34

[6] Brown R and Uhlmann G 1997 Uniqueness in the inverse conductivity problem for nonsmooth conductivities in two dimensions *Commun. Partial Differ. Eqns* **22** 1009–27

[7] Bukhgeim A L 2008 Recovering a potential from Cauchy data in the two-dimensional case *J. Inverse Ill-posed Problems* **16** 19–33

[8] Calderón A P 1980 On an inverse boundary value problem *Seminar on Numerical Analysis and its Applications to Continuum Physics* ed W H Meyer and M A Raupp (Rio de Janeiro: Sociedade Brasileira de Matemática) pp 65–73

[9] Cheney M, Isaacson D and Newell J C 1999 Electrical impedance tomography *SIAM Rev.* **41** 85–101

[10] Francini E 2000 Recovering a complex coefficient in a planar domain from the Dirichlet-to-Neumann map *Inverse Problems* **16** 107

[11] Hamilton S, Herrera C N L, Mueller J and Von Herrmann A 2012 A direct D-bar reconstruction algorithm for recovering a complex conductivity in 2D *Inverse Problems* **28** 095005

[12] Harrach B and Seo J K 2009 Detecting inclusions in electrical impedance tomography without reference measurements *SIAM J. Appl. Math.* **69** 1662–81

[13] Harrach B, Seo J K and Woo E J 2010 Factorization method and its physical justification in frequency-difference electrical impedance tomography *IEEE Trans. Med. Imaging* **29** 1918–26
[14] Harrach B and Seo J K 2010 Exact shape-reconstruction by one-step linearization in electrical impedance tomography *SIAM J. Math. Anal.* **42** 1505–15180
[15] Holder D 2005 *Electrical Impedance Tomography: Methods, History and Applications* (Bristol: Institute of Physics Publishing)
[16] Kim S, Lee J, Seo J K, Woo E J and Zribi H 2008 Multifrequency trans-admittance scanner: mathematical framework and feasibility *SIAM J. Appl. Math.* **69** 22–36
[17] Kim S, Seo J K and Ha T 2009 A nondestructive evaluation method for concrete voids: frequency differential electrical impedance scanning *SIAM J. Appl. Math.* **69** 1759–71
[18] Kim S 2012 Assessment of breast tumor size in electrical impedance scanning *Inverse Problems* **28** 025004
[19] Kim S, Lee E J, Woo E J and Seo J K 2012 Asymptotic analysis of the membrane structure to sensitivity of frequency-difference electrical impedance tomography *Inverse Problems* **28** 075004
[20] Kim S and Tamasan A 2013 On a Calderón problem in frequency differential electrical impedance tomography *SIAM J. Math. Anal.* **45** 2700–9
[21] Knudsen K 2003 A new direct method for reconstructing isotropic conductivities in the plane *Physiol. Meas.* **24** 391–401
[22] Knudsen K and Tamasan A 2004 Reconstruction of less regular conductivities in the plane *Commun. Partial Differ. Eqns* **29** 361–81
[23] Knudsen K, Lassas M, Mueller J and Siltanen S 2009 Regularized D-bar method for the inverse conductivity problem *Inverse Problems Imaging* **3** 599–624
[24] Knudsen K, Lassas M, Mueller J and Siltanen S 2007 D-bar method for electrical impedance tomography with discontinuous conductivities *SIAM J. Appl. Math.* **67** 893–913
[25] Kohn R V and Vogelius M 1984 Determining conductivity by boundary measurements *Commun. Pure Appl. Math.* **37** 113–23
[26] Nachman A 1988 Reconstructions from boundary measurements *Ann. Math.* **128** 531–76
[27] Nachman A 1996 Global uniqueness for a two-dimensional inverse boundary value problem *Ann. Math.* **143** 71–96
[28] Nour S, Mangnall Y F, Dickson J A, Johnson A G and Pearse R G 1995 Applied potential tomography in the measurement of gastric emptying in infants *J. Pediatr. Gastroenterol. Nutr.* **20** 65–72
[29] Pethig R 1987 Dielectric properties of biological materials *Clin. Phys. Physiol. Meas.* A **8** 5–12
[30] Siltanen S, Mueller J and Isaacson D 2000 An implementation of the reconstruction algorithm of A Nachman for the 2D inverse conductivity problem *Inverse Problems* **16** 681–99
[31] Scholz B and Anderson R 2000 On electrical impedance scanning: principles and simulations *Electromedica* **68** 35–44
[32] Schwan H P and Kay C F 1957 The conductivity of living tissue *Ann. New York Acad. Sci.* **65** 1007–13
[33] Seo J K, Lee J, Kim S W, Zribi H and Woo E J 2008 Frequency-difference electrical impedance tomography (fdEIT): algorithm development and feasibility study *Physiol. Meas.* **29** 929–44
[34] Seo J K, Harrach B and Woo E J 2009 Recent progress on frequency difference electrical impedance tomography *ESAIM Proc.* **26** 150–61
[35] Somersalo E, Cheney M and Isaacson D 1992 Existence and uniqueness for electrode models for electric current computed tomography *SIAM J. Appl. Math.* **52** 1023–40
[36] Stojadinovic A *et al* 2005 Electrical impedance scanning for the early detection of breast cancer in young women: preliminary results of a multicenter prospective clinical trial *J. Clin. Oncol.* **23** 2703–15
[37] Sylvester J and Uhlmann G 1987 A global uniqueness theorem for an inverse boundary value problem *Ann. Math.* **125** 153–69
[38] Tidswell T, Gibson A, Bayford R H and Holder D S 2001 Three-dimensional electrical impedance tomography of human brain activity *NeuroImage* **13** 283–94
[39] Uhlmann G 2009 Electrical impedance tomography and Calderón's problem *Inverse Problems* **25** 1–39